Cavitation due to an impacting sphere

K L de Graaf, P A Brandner, B W Pearce and J Y Lee

Australian Maritime College, University of Tasmania, Launceston, Tasmania, Australia 7250

E-mail: kdegraaf@amc.edu.au

Abstract. Cavitation associated with the impact of a sphere on a flat surface is investigated using high-speed photography. The sphere, of diameter 15 or 45 mm and made from Ertacetal® or stainless steel, was fully submerged and accelerated using a spring-loaded mechanism to achieve Reynolds numbers based on impact velocity and sphere radius of up to 7.2×10^4. The static pressure and impact velocity were varied to achieve cavitation numbers ranging from 8.9 to 120.9. High-speed photography of the impacting sphere and induced cavitation bubble was filmed at 105-140 kHz. A log law relationship was found between the non-dimensional maximum bubble radius and the cavitation number. The relationship was modulated by the material properties. Interaction between the sphere and the bubble was also noted.

1. Introduction

Cavitation induced by impact forces is of interest for basic research into inception and has been the subject of many studies. Kleine *et al.* [1] dropped glass and stainless steel spheres onto a submersed target and used Schlieren photography to identify pressure waves in the water which were assumed to be the cause of cavitation. Marston *et al.* [2] dropped stainless steel spheres onto a glass plate covered in a film of liquid. Estimates of the tensile stress for onset of cavitation compared well to the maximum tension criterion proposed by Joseph [3]. Seddon *et al.* [4] observed vapour cavities using high-speed imaging during approach of a steel ball onto a liquid covered glass plate. Uddin *et al.* [5] also used high-speed imaging, and particle tracking, to investigate squeeze flow around a sphere impacting a non-Newtonian film covered plate. High shear regions led to significant viscosity reduction which may have increased sphere penetration into the film and induced cavitation on sphere rebound. Mansoor *et al.* [6] investigated dropping a tungsten carbide sphere onto a liquid covered glass surface, but were not able to reproduce results of Seddon *et al.* [4] of cavitation forming before impact. In nature, cavitation occurs after impact of the raptorial appendage of a peacock mantis shrimp (*Odontodactylus scyllarus*), which can generate forces up to 1501 N at peak speeds of 14-23 m/s, aiding the shrimp's attack on its prey.

The majority of investigations published on cavitation due to impacting spheres involve an initial approach of the sphere through air before entering the liquid. The present study is undertaken in a fully immersed environment, with the sphere accelerated towards the plate with a velocity greater than free-fall.

2. Experimental Setup

The experiments were performed in the variable-pressure Bubble Dynamics Chamber (BDC) at the Cavitation Research Laboratory (CRL), University of Tasmania. The impact spheres were

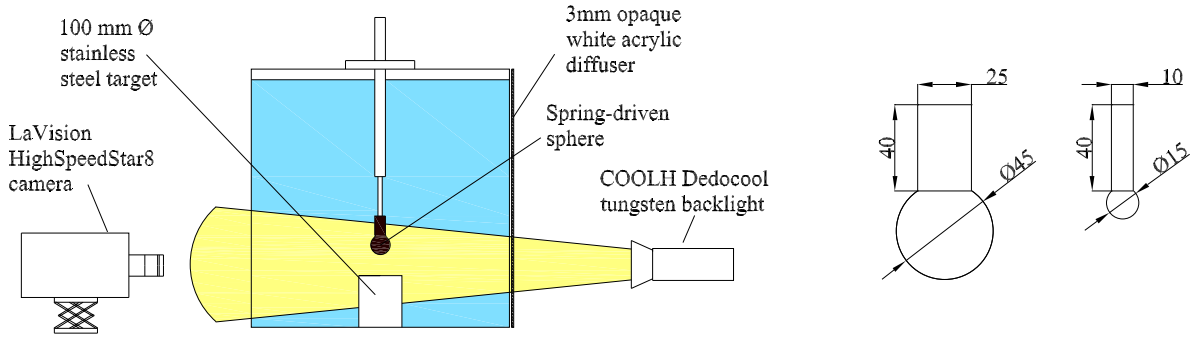

Figure 1: Schematic of the experimental setup showing location of sphere, target, high-speed camera, backlight and diffuser. The compression spring to accelerate sphere is housed within the sphere-tube assembly and not shown. The dimensions of the spheres are shown at right.

15 and 45 mm in diameter, constructed of Ertacetal® plastic and stainless steel. Each in turn were attached to a lightweight rod, fitted to a spring-loaded mechanism mounted in the top of the BDC. The spheres were accelerated into a 100 mm diameter stainless steel target located on the BDC floor at Reynolds numbers, $Re = UR_S/\nu$, ranging from 1.3 to 7.2×10^4 (or up to $U = 3.2$ m/s for 45 mm spheres and 5 m/s for 15 mm spheres), where U is the impact velocity, R_S the sphere radius and ν the kinematic viscosity of water. Tests were conducted at cavitation numbers, $\sigma = (P - P_v)/(0.5\rho U^2)$, ranging from 8.9 to 120.9, where P is the tank pressure, P_v is the vapour pressure and ρ is the water density. The release of the sphere triggered the acquisition of the high-speed photography taken at 105 kHz (45 mm spheres) and 140 kHz (15 mm spheres). A schematic of the setup and dimensions of the spheres are shown in figure 1 and further detail can be found in [7].

3. Results

Images from the high-speed photography for the 45 mm steel sphere are shown in figure 2. Upon impact, cavitation inception occurs due to the liquid stress/pressure singularity created [3]. The annular bubble grows rapidly in the confined space between the sphere and the target. As the bubble approaches its maximum, small annular protrusions form towards the top and bottom of the bubble. At the bubble maximum radius, surface instabilities are evident. These instabilities are also evident in the forward-lit photo shown in figure 3. As the bubble collapses, an annular re-entrant jet forms. The bubble rebounds a second time and becomes more glassy in nature, as evidenced by the backlighting that can be seen through the bubble. The bubble grows a third time, this time in an elongated vertical shape as the top and bottom of the bubble remains attached to the sphere and target respectively.

Figure 4 shows the displacement of the impacting sphere and growth of the cavitation bubble. Both the sphere displacement, d_S, and bubble radius, R, are non-dimensionalised based on the sphere radius, R_S. Time, t, is non-dimensionalised on the first bubble period, T_B, and sphere displacements have been zeroed at the point of impact. For these cases, the deformation of the spheres was calculated from comparison of high-speed movies with images taken of the sphere at rest. The plastic spheres exhibited a maximum deformation (in the vertical direction) of about $0.03R_S$ for a total period of $0.72T_B$ (15 mm sphere) and $0.01R_S$ for $0.30T_B$ (45 mm sphere). The steel spheres deformed about $0.01R_S$ for $0.61T_B$ (15 mm sphere) and $0.004R_S$ for $0.31T_B$ (45 mm sphere). The magnitude of deformation of the different sized spheres is similar for the same material type; however, the deformation time period is similar for the same sized spheres despite the material. It can also be seen that the rebound of the smaller spheres is affected by the bubble dynamics (for the Ertacetal® sphere this is more evident in other instances, not

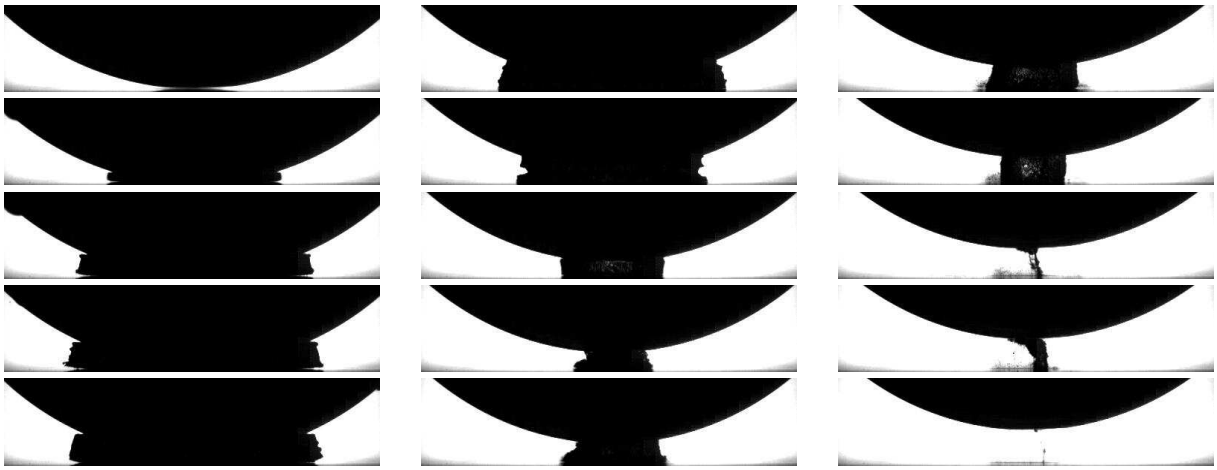

Figure 2: Images of 45 mm stainless steel sphere taken at 105 kHz, every 20^{th} frame shown. Re = 4.0×10^4 (U = 1.8 m/s), σ = 63.74.

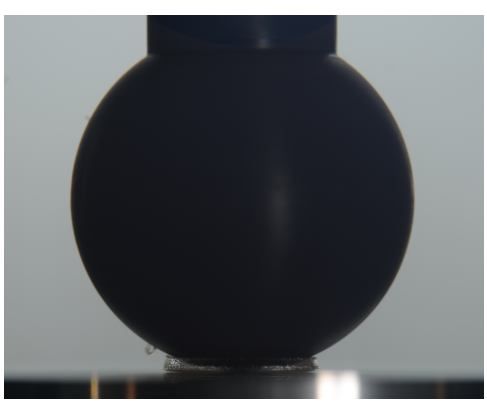

Figure 3: Forward-lit image of the 45 mm Ertacetal® sphere impacting the stainless steel target (left) and an enlarged view of the cavitation (above). Surface instabilities are evident at the vapour-water interface. From comparison with high-speed shadowograph movies, the bubble is in its first growth phase.

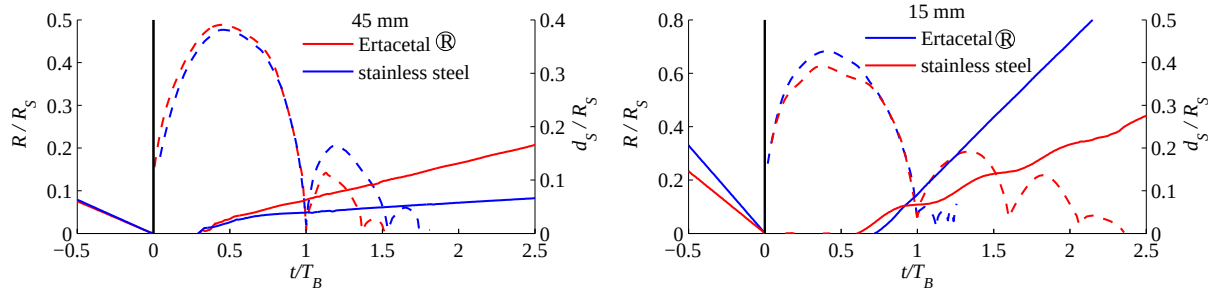

Figure 4: Displacement of sphere and growth of cavitation bubble. 45 mm stainless steel sphere: Re = 5.1×10^4 (U = 2.3 m/s), σ = 37.9. 45 mm Ertacetal® sphere: Re = 5.4×10^4 (U = 2.4 m/s), σ = 35.37. 15 mm stainless steel sphere: Re = 2.6×10^4 (U = 3.4 m/s), σ = 20.3. 15 mm Ertacetal® sphere: Re = 3.1×10^4 (U = 4.4 m/s), σ = 11.7.

plotted here). The 45 mm spheres are largely unaffected by the bubble dynamics, presumably due to the larger inertia.

Figure 5 shows R_{max}/R_S against σ. A log law relationship is evident. A line of best fit for each data set gives a difference in gradient (on the semi-log plot) of approximately 3% and a vertical offset of 0.08. The difference does not change substantially when σ is calculated using the rebound velocity, suggesting that the sphere deformation accounts for the difference in the

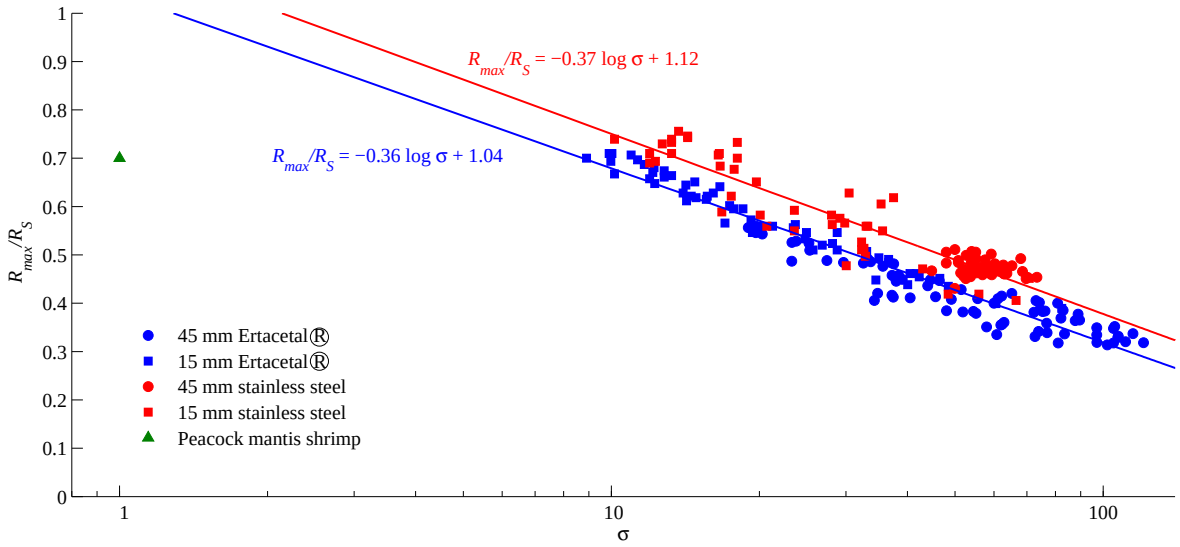

Figure 5: Non-dimensional maximum bubble radius, R_{max}/R_S vs. cavitation number, σ. Peacock mantis shrimp data calculated from Fig. 1 of [8].

maximum bubble radius produced by the Ertacetal® and stainless steel spheres for the same σ. The bubble formed by a peacock mantis shrimp, calculated from Fig. 1 of [8] (assuming the shrimp is not at great depth) is smaller than those produced here. This may be attributable to the difference in material properties of the dactyl heel. Changes in bubble dynamics may also be affected by the differences in seawater due to chemical properties and contaminants affecting surface tension [9].

4. Conclusions

Cavitation produced after impact, in analogy with the mantis shrimp strike, has been investigated using two materials at various cavitation and Reynolds numbers in fully submerged conditions. The maximum dimensionless radius of the cavitation bubble produced scales with a log law relationship with the cavitation number. The offset in radius vs. cavitiation number relationship between the two sphere materials suggests there are other factors (such as material compressibility) that affect the cavitation bubble dynamics, with the more compliant material producing a smaller bubble. Shockwaves in both the liquid and solid media may have an influence and experiments incorporating the schlieren technique are planned to investigate this aspect. There is evidence for the bubble dynamics influencing the sphere rebound, which is more prevalent for the smaller spheres.

References

[1] Kleine H, Tepper S, Takehara K, Etoh T G and Hiraki K 2009 Cavitation induced by low-speed underwater impact *26th International Symposium on Shock Waves* vol 1 (Göttingen, Germany)
[2] Marston J O, Yong W, Ng W K, Tan R B H and Thoroddsen S T 2011 *Exp. Fluids* **50** 729–746
[3] Joseph D D 1998 *J. Fluid Mech.* **366** 367–378
[4] Seddon J R T, Kok M P, Linnartz E C and Lohse D 2012 *Europhys. Lett.* **97** 24004
[5] Uddin J, Marston J O and Thoroddsen S T 2012 *Phys. Fluids* **24** 073104
[6] Mansoor M M, Uddin J, Marston J O, Vakarelski I U and Thoroddsen S T 2014 *Exp. Fluids* **55** 1648
[7] de Graaf K L, Brandner P A, Lee J Y and Pearce B W 2014 Cavitation about a sphere impacting a flat surface *19th AFMC* (Melbourne, Australia)
[8] Patek S N and Caldwell R L 2005 *J. Exp. Bio.* **208** 3655–3664
[9] Chanson H, Aoki S and Hoque A 2006 *J. Coast. Res.* **22** 664–677